# Twisting and Reverse Magnetic Field Effects on Energy Conversion of Magnetostrictive Wire Metal Matrix Composites



doi: 10.1002/pssr.202000281

# Twisting and Reverse Magnetic Field Effects on Energy Conversion of Magnetostrictive Wire Metal Matrix Composites

Zhenjun Yang[1], Zhenjin Wang[1], Manabu Seino[2], Daisuke Kumaoka[2], Go Murasawa[2], Fumio Narita[3a)]

[1] Department of Materials Processing, Graduate School of Engineering, Tohoku University, Sendai 980-8579, Japan

[2] Department of Polymer Science and Engineering, Yamagata University, 4-3-16 Jonan, Yonezawa 992-8510, Yamagata, Japan

[3]Department of Frontier Sciences for Advanced Environment, Graduate School of Environmental Studies, Tohoku University, Sendai 980-8579, Japan

a) corresponding author: narita@material.tohoku.ac.jp

## Abstract

Lightweight metal matrix composites have attracted a great attention for their technological application such as aerospace, automotive, or sporting goods, and the multifunctionality of these composites will further expand the range of applications. In this work, a kind of lightweight 1-3 magnetostrictive FeCo/AlSi composites was investigated to evaluate the effects of the specific structure design and reverse magnetic field on energy conversion under compression. The microstructure of the FeCo/AlSi composite before compression was observed, and the results indicate that there is a great bonding interface, which has the benefits of the strain/stress transfer. Compared with the FeCo/AlSi composite with straight FeCo wire, a design with the twisted FeCo wire significantly enhances the output performance of the magnetostrictive FeCo/AlSi composite. On the other hand, the comparison of the output voltage for the FeCo/AlSi composite in the N-S model (forward magnetization) and N-N model (reverse magnetization) reveals that the reverse magnetization can improve the efficiency of the energy conversion notably. In addition, the results of the output voltage in the theoretical calculation are virtually consistent with that in practical measurement. This research not only proposes a relatively accurate theoretical analysis on the output performance of the FeCo/AlSi composite but also offers a feasible design for further improve the efficiency of the energy conversion for the magnetostrictive wire metal matrix composites.

composite design; twisted FeCo wire; metal matrix composites; magnetostrictive properties; energy harvesting

## Introduction

Magnetostrictive materials have been gaining noteworthy consideration in sensors, actuators and energy harvesters following the development of the Internet of Things (i.e., IoT). In particular, traditional power supplies such as batteries are characterized by several disadvantages of recharge and short lifespan, which are inevitable to hinder the further technical revolution in this field [1-3]. There are a series of imminent challenges that not only solve the power supplies with long-lasting lifetime and miniaturization but also improve the performance of sensors and actuators with high sufficient energy conversion, signal transmission and stability [4, 5]. The magnetostrictive materials that have been widely studied over the last decades offer a promising alternative for solving these problems. Following the development and improvement in processing technique and composition change, many magnetostrictive materials including their composites with excellent magnetostrictive properties have been successfully fabricated, which provides expecting feasibility for these materials that were employed in smart detective components and self-powered microsystems [6, 7].

Several primary magnetostrictive materials have been systematically investigated, such as TbDyFe alloy (Terfenol-D), FeGa alloy (Galfenol), iron-cobalt alloy (FeCo), etc. Terfenol-D is considered as a promising candidate in sensors, actuators and energy harvesters at the beginning, because of its excellent magnetostriction. However, the extreme brittleness and low cost-effectiveness constrain its further large-scale application, especially in portable equipment. To solve those problems, a series of polymer-matrix composite doped by Terfeno-D were prepared [8-11]. The ductility of these composites indeed has an improvement in a way but at the expense of the dramatic decrease in magnetostrictive properties. In addition, the rare-element-dependent feature for Terfenol-D is difficult to reduce the production cost for wide industrialization. On the other hand, Galfenol alloy has been attracting considerable attention in consideration of its metal-like properties and relatively great magnetostriction [12, 13]. Nevertheless, sophisticated processing is necessary for the Galfenol alloys to obtain the appropriate microstructures and phases. In addition, it is difficult to form this kind of material into certain specific sizes, especially for thin plates and wires. Considering the relatively high cost of raw materials, Galfenol alloy is unsuitable in widespread industrialization, especially for meeting the requirement of miniaturized components.

FeCo alloys are good candidates for energy harvesting materials due to their advantages of low cost and abundance compared to those of Terfenol-D and Galfenol although the magnetostriction is small [14]. In addition, FeCo alloys exhibit high strength, ductility, and excellent workability, allowing easy fabrication of FeCo wires. In recent years, it was shown that the embedding of the FeCo wires in a polymer matrix leads to magnetostrictive composite materials with enhanced inverse magnetostrictive effect [15-19].

All of the above-mentioned studies have focused on composite materials in which magnetostrictive FeCo wires are embedded in the epoxy alloy matrix. On the other hand, lightweight metal matrix composites have received wider attention in modern industries due to their outstanding properties including low density and high strength. To the author's knowledge, very little research has been done on the design and evaluation of lightweight metal matrix composites with inverse magnetostrictive effect.

The majority of researchers has been focusing on the composite design and composition change to improve the magnetostrictive and/or comprehensive properties in recent years. However, these methods only obtain limited improvement but at the expense of a reduction in several primary properties and an increase in the cost of raw materials and processing. In contrast, certain appropriate structural design can obtain relatively great magnetostrictive properties or energy-harvesting performance, even using common materials. It has been reported [20] that localized stress concentration introduced by a notch-like structure has the benefits of amplifying the energy conversion or magnetostrictive properties. Besides, a multilayered composite involving positive and negative magnetostrictive materials can enhance the magnetostrictive properties for each other [21].

In this study, a magnetostrictive material FeCo, which has comparable magnetostriction to Galfenol alloy but greater machining properties and cost-effectiveness, is employed. A lightweight magnetostrictive wire metal matrix composite is fabricated, and the effects of specific structure and reverse magnetization on the mechanical-magnetic energy conversion are then systematically investigated. The advantage of this study is that it provides magnetostrictive functionality with a very

small amount of FeCo wire to maintain the lightweight of the composites. Combing with the finite element analysis (i.e., FEA), this work aims to offer a calculation method to predict the efficiency of energy conversion. This work can not only provide insights into the mechanism responsible for the mechanical-magnetic energy conversion but also offer a particular design concept for further improving the magnetostrictive properties or harvesting energy performance.

## Experimental procedure

A class of lightweight magnetostrictive wire composite was prepared in this work. The abundant $Fe_{30}Co_{70}$ at% alloy is employed, which has the comparable magnetostriction to Galfenol alloys but greater comprehensive properties. The matrix of the composite is a kind of AlSi alloy (i.e., AC3A, Japanese industrial standards, see Table 1). To fabricate the composite, initially, the FeCo wires with a diameter of 0.5 mm, after undergoing hot- and cold-rolling, were embedded into the AlSi metal liquid under a compression 22 MPa at 700 ℃ for 1 hour. Following this, the composite was solidified at an Ar protective atmosphere until room temperature, and the entire cooling process is approximately 1 hour. Eventually, the FeCo/AlSi composite underwent a cooling treatment in the air for about 30 minutes. The final FeCo/AlSi composite was processed into a cylinder with a diameter of 10 mm and a length of 40 mm. According to several previous studies [20, 22, 23], a specific shape for magnetostrictive materials has the benefits to enhance the efficiency of energy conversion. Therefore, it should be noted here that the employed FeCo wires are not the straight but twisted shape, as shown in Fig. 1(a). The experimental samples and twisted FeCo wires are shown in Fig. 1(b). The relevant variables such as the volume fraction, cross-sectional area of the FeCo wires with the whole composite are listed in Table 2, where the superscript f represents the FeCo wire. Here the volume fraction of the twisted FeCo wire is 0.025 in the composite. It is quite low. This is because the purpose of this work is to make a light Al alloy have an inverse magnetostrictive effect with a small amount of FeCo wire. For the composite with the straight FeCo wires, the effect of volume fraction on the energy conversion was discussed in detail [23].

Fig. 2 (a) illustrates the schematic for the energy harvesting setup during compression. The pickup coil with $1.1 \times 10^5$ turns and 6.11 kΩ was connected with a data logger to determine the output voltage

in response to the compression. The experiment of energy conversion was conducted in a uniaxial cyclic compression for the FeCo/AlSi magnetostrictive composite at five times as shown in Fig. 2(b). The compressing load was controlled at constant crosshead velocities of $d\delta/dt$ = 0.25, 0.5, 0.75, 1.0 and 2.0 mm/s, where $\delta$ and $t$ represent the crosshead displacement and experimental time, respectively. Two distinct bias magnetic fields of 365 and 495 mT provided by the external magnets were used in this work to examine the effect of bias magnetic field on the output performance. Here, it must be emphasized that the magnetization mode for the bias magnetic field is classified into N-S (forward magnetization) and N-N (reverse magnetization), respectively. In more detail, N and S denote the magnetic pole within the magnets. The difference in these two modes is the specific magnetic poles of the magnets which are connected with the FeCo /AlSi composite. On the other hand, in view of the process of solidification for the FeCo/AlSi, the element analysis and microstructure observation were carried out through the energy-dispersive detector (EDS) and scanning electron microscopy (SEM), respectively.

## Theoretical calculation

Theoretical analysis is employed in this work to provide insights into the explanation of the energy conversion during compression for the magnetostrictive FeCo/AlSi composite. In general, an accurate theoretical model, especially in the quantitative calculation, is beneficial to offer feasible and time-saving guidance not only for composite design but also for performance prediction. To enable the calculation of the energy-conversion performance for the FeCo/AlSi composite, two constitutive equations describing the mechanism of mechanical-magnetic conversion is given as follows [24, 25]:

$$\varepsilon = s\sigma + d'H, \tag{1}$$

$$B = d'\sigma + \mu H, \tag{2}$$

where $\sigma$ and $\varepsilon$ denote the stress and strain, $B$ and $H$ represent the magnetic induction and magnetic field intensity, and $s$, $d'$ and $\mu$ are the elastic compliance, magnetoelastic constant and magnetic permeability, respectively. On the other hand, the effect of residual stress on energy conversion has also been taken into account in view of the specific structure of FeCo wires and thermal treatment. The magnetoelastic constant is therefore can be further described by

$$d' = d + (m + r\sigma_0)H, \tag{3}$$

where $d$ is the piezo-magnetic constant, and the constant $m$ denotes the magnetostrictive strain produced by per unit external magnetic field. The symbol $r$ is a constant that physically denotes the coupling magnetostrictive strain produced by per unit external magnetic field under per unit internal stress [23, 26]. In addition, $\sigma_0$ represents the residual stress within the FeCo wire.

The Rectangular Cartesian coordinates $x_i$ (O-$x_1$, $x_2$, $x_3$) are utilized here, and the easy axis to be magnetized for the FeCo wire is assumed along with $x_3$-direction, namely, the direction of length. In this case, the longitudinal magnetostrictive deformation mode (33) is primary [27]. Thus, the $x_3$-component of the magnetic field intensity is virtually responsible for the whole variation of the magnetoelastic constant during compression. As a sequence, the three-dimension model can be simplified as a one-dimensional model only along the $x_3$-direction. Hence, the constitutive equations can be rewritten by the following equations:

$$\varepsilon_{33}^{\mathrm{f}} = s_{33}^{\mathrm{f}}\sigma_{33}^{\mathrm{f}} + \{d_{33}^{\mathrm{f}} + (m + r\sigma_0)H_3^{\mathrm{f}}\}H_3^{\mathrm{f}}, \tag{4}$$

$$B_3^{\mathrm{f}} = \{d_{33}^{\mathrm{f}} + (m + r\sigma_0)H_3^{\mathrm{f}}\}\sigma_{33}^{\mathrm{f}} + \mu_{33}^{\mathrm{f}}H_3^{\mathrm{f}}, \tag{5}$$

where $\varepsilon_{33}^{\mathrm{f}}$, $\sigma_{33}^{\mathrm{f}}$ are the components of strain and stress tensor, $B_3^{\mathrm{f}}$ and $H_3^{\mathrm{f}}$ denote the components of magnetic induction and magnetic field intensity vectors, and $s_{33}^{\mathrm{f}}$, $d_{33}^{\mathrm{f}}$ and $\mu_{33}^{\mathrm{f}}$ are the elastic compliance, piezo-magnetic constant and magnetic permeability, respectively. In general, it is commonly believed that the bias magnetic field $H_0 = B_0/\mu_0$, where $\mu_0 = 1.26 \times 10^{-6}$ H/m is the magnetic permeability of free space, is far greater than the induced magnetic field intensity stemming from the inverse magnetostrictive effect. As a result, the equations (4) and (5) can be described as follows:

$$\varepsilon_{33}^{\mathrm{f}} = s_{33}^{\mathrm{f}}\sigma_{33}^{\mathrm{f}} + d_{33}^{\mathrm{f}}\left(\frac{B_0}{\mu_{33}^{\mathrm{f}}}\right) + (m + r\sigma_0)\left(\frac{B_0}{\mu_{33}^{\mathrm{f}}}\right)^2, \tag{6}$$

$$B_3^{\mathrm{f}} = d_{33}^{\mathrm{f}}\sigma_{33}^{\mathrm{f}} + (m + r\sigma_0)\left(\frac{B_0}{\mu_{33}^{\mathrm{f}}}\right)\sigma_{33}^{\mathrm{f}} + B_0, \tag{7}$$

Here, the strain tensor component $\varepsilon_{33}^{\mathrm{m}}$ and magnetic induction vector component $B_3^{\mathrm{m}}$ of the AlSi matrix are given by

$$\varepsilon_{33}^{\mathrm{m}} = s_{33}^{\mathrm{m}}\sigma_{33}^{\mathrm{m}}, B_3^{\mathrm{m}} = \mu_0 H_3^{\mathrm{m}}, \tag{8}$$

where the superscript m denotes the AlSi matrix. Following this, it is assumed that there is a perfect bonding interface between the FeCo wire and AlSi matrix, namely, $s_{33}^{\mathrm{f}} = s_{33}^{\mathrm{m}}$. Besides, the components of the stress tensors of the FeCo wire and AlSi matrix are uniform in consideration of the transverse isotropy of the representative volume element in calculation. The mean stress $\sigma_{33}^{0}$ is therefore can be described by

$$\sigma_{33}^{0} = \sigma_{33}^{\mathrm{f}} v^{\mathrm{f}} + \sigma_{33}^{\mathrm{m}}(1 - v^{\mathrm{f}}), \tag{9}$$

Here, the $\sigma_{33}^{0}$ is equivalent to the stress imposed by the compression on the FeCo/AlSi composite cylinder. As a result, the output voltage of the composite can be calculated through the following equations:

$$V_{\mathrm{out}} = -NA^{\mathrm{f}} \frac{\mathrm{d}B_3^{\mathrm{f}}}{\mathrm{d}t} = -NA^{\mathrm{f}} \frac{s_{33}^{\mathrm{m}}}{s_{33}^{\mathrm{m}} v^{\mathrm{f}} + s_{33}^{\mathrm{f}}(1 - v^{\mathrm{f}})} \{d_{33}^{\mathrm{f}} + \frac{(m + r\sigma_0)}{\mu_{33}^{\mathrm{f}}} B_0\} \frac{\mathrm{d}\sigma_{33}^{0}}{\mathrm{d}t}, \tag{10}$$

where *N* denotes the turns of the pickup coil. The main properties of the FeCo wire and AlSi matrix used in this simulation have been listed in Table 3. The residual stress $\sigma_0$ within the FeCo wire can be calculated by three-dimensional FEA. The three-dimensional constitutive equations and the relevant properties of FeCo alloy associated with the calculation for FEA can be found in Ref. [20].

## Results and discussion

The SEM observation and EDS element analysis for the magnetostrictive FeCo/AlSi composite were performed to characterize the interface between FeCo and AlSi that plays a vital impact on the energy conversion. Fig. 3(a) illustrates that the interface between these two alloys has a zigzag boundary, which has the benefits of strain/stress transfer, even enhance the stress concentration along with the interface. As described above, stress concentration can intensify the magnetic induction variation in a way, namely, it can improve the efficiency of energy conversion significantly. On the other hand, combining with the EDS element analysis (see Fig. 3(b)), it is evident to identify the presence of the element diffusion around the interface of the FeCo and AlSi alloys. As a result, it is reasonably

believed that there is a great bonding interface between the FeCo wire and AlSi matrix both in physical and chemical.

The comparison of the output performance of the composites with the twisted and straight FeCo wires for the N-S model is shown in Fig. 4(a), which plots the output voltage $V_{out}$ versus velocity $d\delta/dt$. Here, it must be emphasized that these two kinds of composites have identical dimensions, such as sample diameter, sample length and FeCo volume. It is obvious that the composite with the twisted FeCo wires has a greater output performance than that with the straight FeCo wires. This phenomenon is attributed to the localized stress concentration around the FeCo and AlSi interface that leads to a faster variation in magnetic induction, then giving rise to the greater output voltage. On the other hand, differing from the common magnetization model N-S, the N-N magnetization model is proposed in this work to analyze the effects of the magnetization direction on the output performance. It should be noted here that the employed sample is only the composite with the twisted FeCo wires in this comparison. Fig. 4(b) indicates that the output voltage of the FeCo/AlSi composite in the N-N model is far greater than that in the common N-S model at every crosshead velocities. According to the common consensus, the bias magnetic field in the N-N model is lower than that in the N-S model. It seems that the lower bias magnetic field is responsible for this phenomenon. To identify the assumption mentioned above, the output voltages of the FeCo/AlSi composite (twisted FeCo wires) at different bias magnetic fields are compared, as shown in Fig. 4(c). It reveals that the output voltage of the FeCo/AlSi composite at the powerful bias magnetic field is greater than that at the weak bias magnetic field. Namely, the lower bias magnetic field is not the real reason resulting in the greater output voltage in the N-N model. Besides, it can be also observed that the increments of the output voltage in the N-S and N-N models at different crosshead velocities decline with the increasing crosshead velocities, see Fig. 4(d).

To enable a better understanding of the difference in the output voltage between the N-S and N-N models, it is necessary to identify the mechanism responsible for the magnetic induction variation related to the output voltage. In general, the magnetic induction variation stems from the rotation of the magnetic domain and/or the motion of the magnetic domain wall. As a result, the change of magnetic domain within the FeCo/AlSi composite under compression is crucial for the analysis with regard to the mechanism on this phenomenon. Fig. 5 illustrates the difference in domain rotation in N-S and N-N models. Here, the arrows in these figures show the magnetic induction vector. The bias

magnetic field in the N-S model always forces the inner magnetic domain to rotate to an identical unidirectional. However, in the N-N model, the magnetization within the composite, especially close to the surface of the magnet, exhibits reverse magnetization direction. In the powerful area of the bias magnetic field, an area close to the surface of the magnet, there is usually no obvious difference for the FeCo/AlSi composite in the magnetic induction variation under compression, even the reverse magnetization. The significant difference appears in the area with relative weak magnetization, namely, the middle parts of the FeCo/AlSi composite. In more detail, the rotation of the magnetic domain always needs the energy to overcome the energy barrier. In addition, the energy barriers for most magnetic domains differ. Even for the same magnetic domain, the energy barriers rotating to the different directions are also different. In this case, the middle area within the FeCo/AlSi composite, magnetized by a relative weak bias magnetic field, shows the difference in magnetization in the N-S and N-N models. First, in the N-S model, because of the energy barrier, the rotations in terms of the N-S direction exhibit different rotation angles deviating from the vertical direction, that is, the magnetization direction. On the other hand, in the N-N model, the middle area, with reverse bias magnetic fields, can offer the optimal rotation direction with the lowest energy barrier for every magnetic domain, among these two directions. Namely, the magnetization angle is more close to the vertical direction for the most magnetic domain within in FeCo/AlSi composite in the N-N model. Besides, the compression always forces the magnetic domain to rotate to the direction that is perpendicular to both the compression and bias magnetic field. During the process, the rotation of the magnetic domain leads to the magnetic induction variation, and then generates the output voltage. In this way, the original magnetization angle, as shown in the insets of Fig. 5, plays a vital role in the output voltage. As a consequence, the reverse magnetic field can provide optimal magnetization among two directions in the N-N model, especially in the middle area within the FeCo/AlSi composites. This is the real reason responsible for the greater output voltage in the N-N model. In addition to the rotation of the magnetic domain, the motion of the magnetic domain wall also results in the magnetic induction variation. It is also can be explained through the energy barrier with respect to the motion of the magnetic domain wall. Namely, the reverse magnetic field has the benefits of the motion of the magnetic domain wall in the optimal direction. Thus, the detailed explanation is omitted here. In conclusion, the reverse magnetic field in the N-N model can lead to the optimal magnetization in the rotation of the magnetic domain and/or the motion of the magnetic domain wall, then giving rise to the greater output voltage, compared with the N-S model. Here, the effects of the reverse magnetic field are referred to as the residual magnetic field (RMF) enhancement in this work.

A promising approach to calculate the output voltage for the 1-3 magnetostrictive FeCo/AlSi composite is also proposed in this study. Here, a comparison of the output voltages for the FeCo/AlSi composite in calculation and measurement is shown in Fig. 6. According to the equation (10), the residual stress $\sigma_0$ of approximately $4.18 \times 10^5$ Pa within the FeCo wires before compression has been considered through the FEA (see Appendix) and the corresponding coefficient $r$ is about $2.73 \times 10^{-19}$ $m^2$ $A^{-2}$ $Pa^{-1}$. In Fig. 6, the stress-rate $\mathrm{d}\sigma_{33}^0/\mathrm{d}t$ is used to evaluate the output voltage in terms of the equation (10). The dashed line here represents the results of the output voltage in the calculation, which is virtually in great agreement with that in measurement in the N-S model. However, due to the presence of the RMF enhancement in the N-N model, the results in the N-N model are greater than that both in the calculation and N-S model. As a consequence, it can be well demonstrated that the theoretical calculation can predict the output performance of the magnetostrictive FeCo/AlSi composite, especially in the N-S model.

## Conclusions

A kind of lightweight 1-3 magnetostrictive FeCo/AlSi composite with the twisted FeCo wires was fabricated in this study. The relevant microstructure exhibits that there is a great bonding interface both in physical and chemical. A specific design, the twisted FeCo wires, is beneficial to induce the localized stress concentration, then giving rise to a great output performance. A theoretical calculation to predict the output voltage for the FeCo/AlSi composite is also proposed in this work, and it is in good agreement with the results in the N-S model. On the other hand, through the comparison with the common magnetization model N-S, the N-N model for the FeCo/AlSi composite exhibits the greater performance in energy conversion owing to the effect of the reverse magnetic field. In this case, this work not only offers an accurate theoretical calculation for the output performance in the N-S model, but also provides a feasible concept for the design of the magnetostrictive composites to further improve the property of energy conversion with less FeCo wire.

## References


[1] Chen AP, Dai YM, Eshghinejad A, Liu Z, Wang ZC, Bowlan J, et al. Competing Interface and Bulk Effect-Driven Magnetoelectric Coupling in Vertically Aligned Nanocomposites. Adv Sci. 2019;6:1901000.

[2] Zhang B, Jin K, Kou Y, Zheng XJ. The model of active vibration control based on giant magnetostrictive materials. Smart Mater Struct. 2019;28:085028.

[3] Zhang YW, Su C, Ni ZY, Zang J, Chen LQ. A multifunctional lattice sandwich structure with energy harvesting and nonlinear vibration control. Compos Struct. 2019;221:110875.

[4] Domenjoud M, Berthelot E, Galopin N, Corcolle R, Bernard Y, Daniel L. Characterization of giant magnetostrictive materials under static stress: influence of loading boundary conditions. Smart Mater Struct. 2019;28:095012.

[5] Jahjah W, Manach R, Le Grand Y, Fessant A, Warot-Fonrose B, Prinsloo ARE, et al. Thickness dependence of magnetization reversal and magnetostriction in $Fe_{81}Ga_{19}$ thin films. Phys Rev Appl. 2019;12:024020.

[6] Kumar A, Arockiarajan A. Temperature dependent magnetoelectric (ME) response in press-fit FeNi/PZT/Ni self-biased ring composite. J Appl Phys. 2019;126:094102.

[7] Seo HY, Shim IB. Magnetocapacitance of magnetically strained multilayered thin films. J Magn Magn Mater. 2019;481:136-9.

[8] Yoffe A, Shilo D. The magneto-mechanical response of magnetostrictive composites for stress sensing applications. Smart Mater Struct. 2017;26:065007.

[9] Issindou V, Viala B, Gimeno L, Cugat O, Rado C, Bouat S. Fabrication methods for high-performance miniature disks of Terfenol-D for energy harvesting. Sensor Actuat A-Phys. 2018;284:1-5.

[10] Muhammad F, Hu H, Xu HG. Study of magnetoelastic behavior of Terfenol-D under low frequency and low strength magnetic fields for alternating magnetic field measurements. Mater Lett. 2019;240:77-9.

[11] Newacheck S, Youssef G. Synthesis and characterization of polarized novel 0-3 Terfenol-D/PVDF-TrFE composites. Compos Part B-Eng. 2019;172:97-102.

[12] Palacheva VV, Emdadi A, Emeis F, Bobrikov IA, Balagurov AM, Divinski SV, et al. Phase transitions as a tool for tailoring magnetostriction Fe-Ga composites. Acta Mater. 2017;130:229-39.

[13] Bai YL, Jiang N, Zhao SF. Giant magnetoelectric effects in pseudo 1-3 heterostructure films with FeGa nanocluster-assembled micron-scale discs embedded into $Bi_5Ti_3FeO_{15}$ matrices. Nanoscale. 2018;10:9816-21.

[14] Narita F, Fox M. A Review on Piezoelectric, Magnetostrictive, and Magnetoelectric Materials and Device Technologies for Energy Harvesting Applications. Adv Eng Mater. 2018;20:1700743.

[15] Narita F, Inverse Magnetostrictive Effect in $Fe_{29}Co_{71}$ Wire/Polymer Composites. Adv Eng Mater. 2017; 19: 1600586.

[16] Narita F, Katabira K. Stress-Rate Dependent Output Voltage for $Fe_{29}Co_{71}$ Magnetostrictive Fiber/Polymer Composites: Fabrication, Experimental Observation and Theoretical Prediction. Mater. Transactions 2017; 58: 302-304.

[17] Katabira K, Yoshida Y, Masuda A, Watanabe A, Narita F, Fabrication of Fe–Co Magnetostrictive Fiber Reinforced Plastic Composites and Their Sensor Performance Evaluation. Materials 2018; 11: 406.

[18] Katabira K, Kurita H, Yoshida Y, Narita F, Fabrication and Characterization of Carbon Fiber Reinforced Plastics Containing Magnetostrictive Fe-Co Fibers with Damage Self-Detection Capability. Sensors 2019; 19: 4984.
[19] Wang Z, Mori K, Nakajima K, Narita F, Fabrication, Modeling and Characterization of Magnetostrictive Short Fiber Composites. Materials 2020; 13: 1494.
[20] Yang ZJ, Kurita H, Takeuchi H, Katabira K, Narita F. Enhancement of Inverse Magnetostrictive Effect through Stress Concentration for a Notch-Introduced FeCo Alloy. Adv Eng Mater. 2019;21:1800811.
[21] Yang ZJ, Nakajima K, Onodera R, Tayama T, Chiba D, Narita F. Magnetostrictive clad steel plates for high-performance vibration energy harvesting. Appl Phys Lett. 2018;112:073902.
[22] Nakajima K, Kurita H, Narita F. Performance boost of co-rich fe-co based alloy magnetostrictive sensors via nitrogen treatment. Sensor Actuat A-Phys. 2019;295:75-83.
[23] Yang ZJ, Nakajima K, Jiang LX, Kurita H, Murasawa G, Narita F. Design, fabrication and evaluation of metal-matrix lightweight magnetostrictive fiber composites. Mater Design. 2019;175:107803.
[24] Leung CM, Li JF, Viehland D, Zhuang X. A review on applications of magnetoelectric composites: from heterostructural uncooled magnetic sensors, energy harvesters to highly efficient power converters. J Phys D Appl Phys. 2018;51:263002.
[25] Xu XP, Zhang CL, Han QK, Chu FL. Hybrid energy harvesting from mechanical vibrations and magnetic field. Appl Phys Lett. 2018;113:013901.
[26] Wan YP, Fang DN, Hwang KC. Non-linear constitutive relations for magnetostrictive materials. Int J Nonlin Mech. 2003;38:1053-65.
[27] Mori K, Shindo Y, Narita F, Dynamic electromagneto-mechanical behavior of clamped-free giant magnetostrictive/piezoelectric laminates under AC electric fields. Smart Mater. Struct. 2012; 21: 115003.

## Acknowledgements

The authors greatly acknowledge the support of this work by Japan Society for the Promotion of Science (JSPS), KAKENHI Grant Number 19H00733. We would also like to thank Tohoku Steel Co. Ltd. for providing FeCo wire.

## Appendix

The details of the FEA to simulate the residual stress $\sigma_0$ are described below. A three-dimensional FEA is employed here to calculate the residual thermal stress within the FeCo wires during heat treatment, owing to that the thermal residual stress resulting from the varying temperatures has an effect on domain rotation and/or domain wall motion. To correspond to the practical experiment, the simulation procedure is divided into three process: (1) the FeCo/AlSi composite is heated from 25 ℃ to 700 ℃; (2) following this, the specimen is cooled to 25 ℃; (3) finally, remove the protective atmosphere and compressing pressure 22 MPa. The constitutive equation can be expressed as

$$\begin{Bmatrix} \varepsilon_{11}^{j} \\ \varepsilon_{22}^{j} \\ \varepsilon_{33}^{j} \\ 2\varepsilon_{23}^{j} \\ 2\varepsilon_{31}^{j} \\ 2\varepsilon_{12}^{j} \end{Bmatrix} = \begin{bmatrix} s_{11}^{j} & s_{12}^{j} & s_{13}^{j} & 0 & 0 & 0 \\ s_{12}^{j} & s_{11}^{j} & s_{13}^{j} & 0 & 0 & 0 \\ s_{13}^{j} & s_{13}^{j} & s_{33}^{j} & 0 & 0 & 0 \\ 0 & 0 & 0 & s_{44}^{j} & 0 & 0 \\ 0 & 0 & 0 & 0 & s_{44}^{j} & 0 \\ 0 & 0 & 0 & 0 & 0 & s_{66}^{j} \end{bmatrix} \begin{Bmatrix} \sigma_{11}^{j} \\ \sigma_{22}^{j} \\ \sigma_{33}^{j} \\ \sigma_{23}^{j} \\ \sigma_{31}^{j} \\ \sigma_{12}^{j} \end{Bmatrix} + \begin{Bmatrix} \alpha^{j} \\ \alpha^{j} \\ \alpha^{j} \\ 0 \\ 0 \\ 0 \end{Bmatrix} \theta \quad (j = \text{f,m}) \tag{A.1}$$

where $\theta = T - T_{\text{R}}$ is the temperature change for the stress-free reference temperature $T_{\text{R}}$, and $\alpha^{j}$ ($j$ = f, m) is the coefficient of thermal expansion, and $s_{11,}^{j} s_{12,}^{j} s_{13}^{j}, s_{44,}^{j} s_{66}^{j}$ are the elastic compliance. The detailed parameters for these two materials (i.e., FeCo and AlSi) are shown in Table A1.

Table 1 Composition of the AlSi alloy

| Elements | Al | Si | Cu | Mg | Zn | Fe | Mn |
|---|---|---|---|---|---|---|---|
| Wt. % | >80.00 | 10.00 | 0.25 | 0.15 | 0.30 | 0.8 | 0.35 |

Table 2 Relevant parameters of the FeCo/AlSi composites

| Specimen | $v^{f}$ | $A^{f}$ ($mm^2$) | Diameter (mm) | Length (mm) |
|---|---|---|---|---|
| FeCo/AlSi | 0.025 | 1.96 | 10 | 40 |

Note: $v^{f}$ and $A^{f}$ denote the volume fraction and whole cross-sectional area of the FeCo wires.

Table 3 Main simulation parameters of the FeCo wire and AlSi matrix

| $s_{33}^{m}$ ($\times10^{-12}m^2/N$) | $s_{33}^{f}$ ($\times10^{-12}m^2/N$) | $d_{33}^{f}$ ($\times10^{-9}m/A$) | $m$ ($\times10^{-12}m^2/A^2$) | $\mu_{33}^{f}$ ($\times10^{-6}H/m$) | $v^{m}$ |
|---|---|---|---|---|---|
| 13 | 5.5 | 0.125 | 0.0123 | 37.7 | 0.34 |

Note: $v^{m}$ denotes the Poisson's ratio.

Table A1 Relevant calculation parameters of the FeCo wire and AlSi matrix

| Materials | Elastic compliance ($\times10^{-12}\,m^2/N$) | | | | | | Coefficient of thermal expansion α ($10^{-6}/K$) |
|---|---|---|---|---|---|---|---|
| | $s_{11}$ | $s_{33}$ | $s_{44}$ | $s_{66}$ | $s_{12}$ | $s_{13}$ | |
| FeCo | 5.5 | 5.5 | 14.3 | 14.3 | -1.65 | -1.65 | 11.9 |
| AlSi | 13 | 13 | 33.8 | 33.8 | -3.9 | -3.9 | 23.9 |

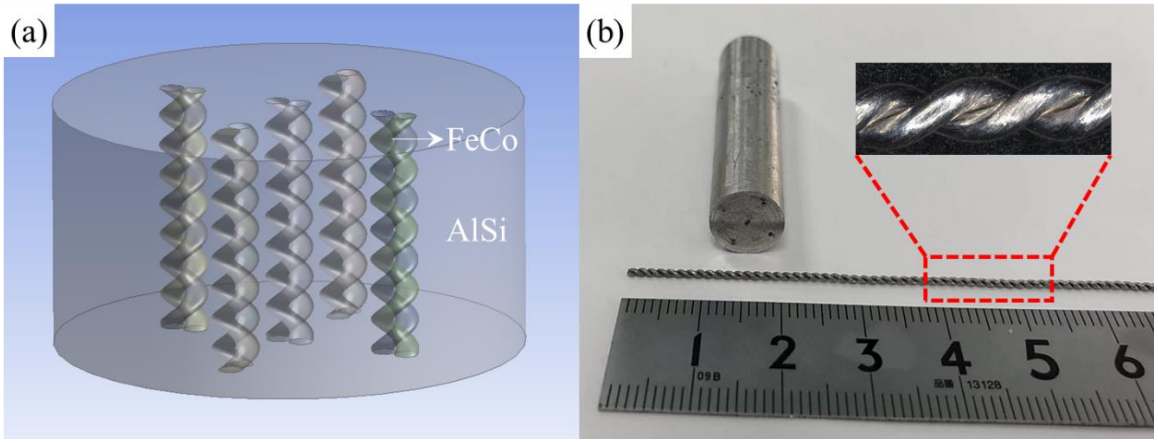


Fig. 1(a) Schematic and (b) photography of the FeCo/AlSi composite

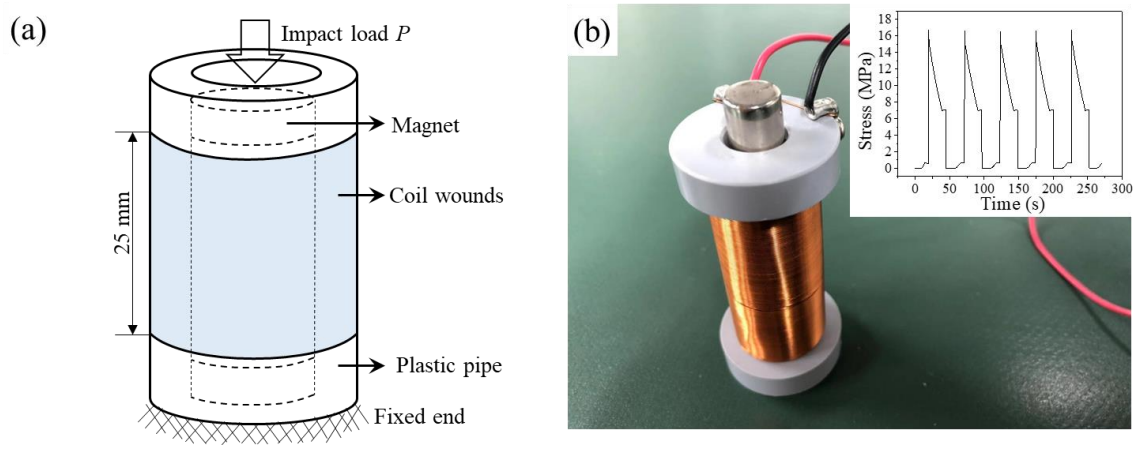


Fig. 2(a)Schematic and (b) physical assembly of the energy harvesting setup under compression

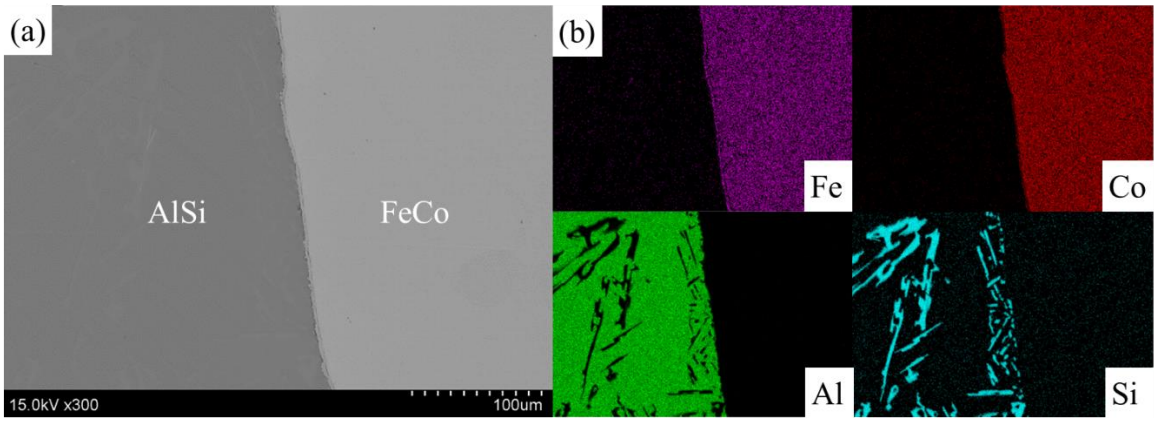


Fig. 3(a) SEM diagram and (b) EDX element analysis of the microstructure for the FeCo/AlSi composite

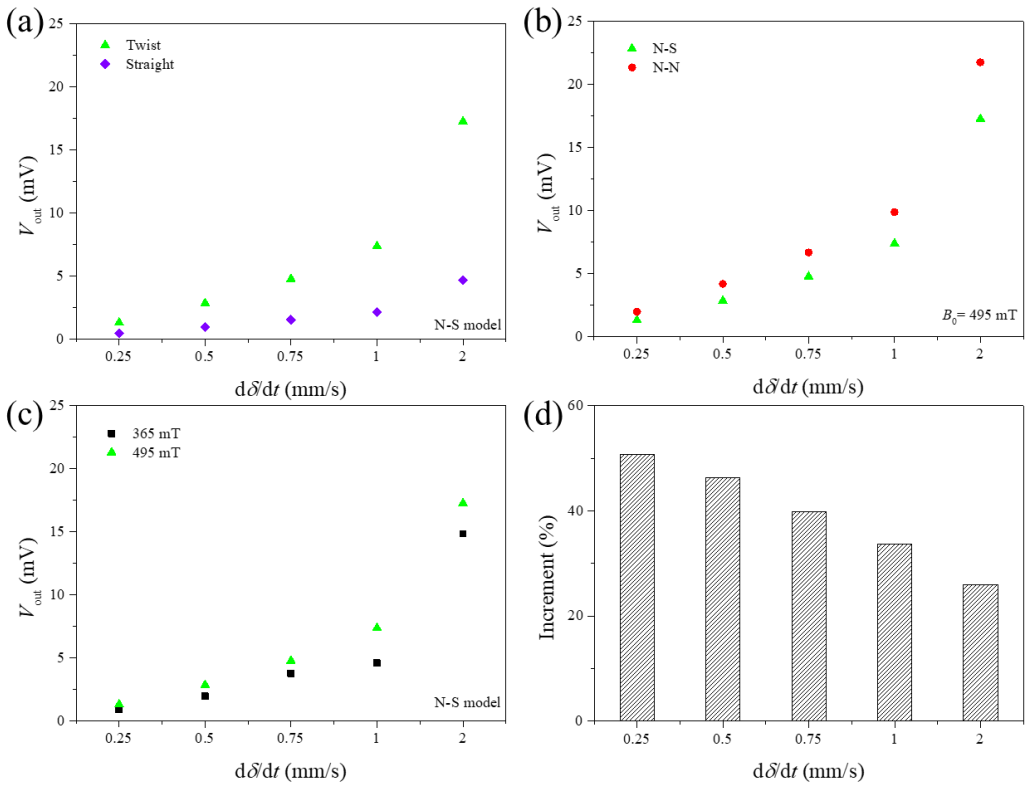


Fig. 4 Comparisons of the output voltage for the FeCo/AlSi composite in different (a) processed FeCo wires, (b) models and (c) bias magnetic fields; (d) Increments of the output voltage at different crosshead velocities between the N-S and N-N models

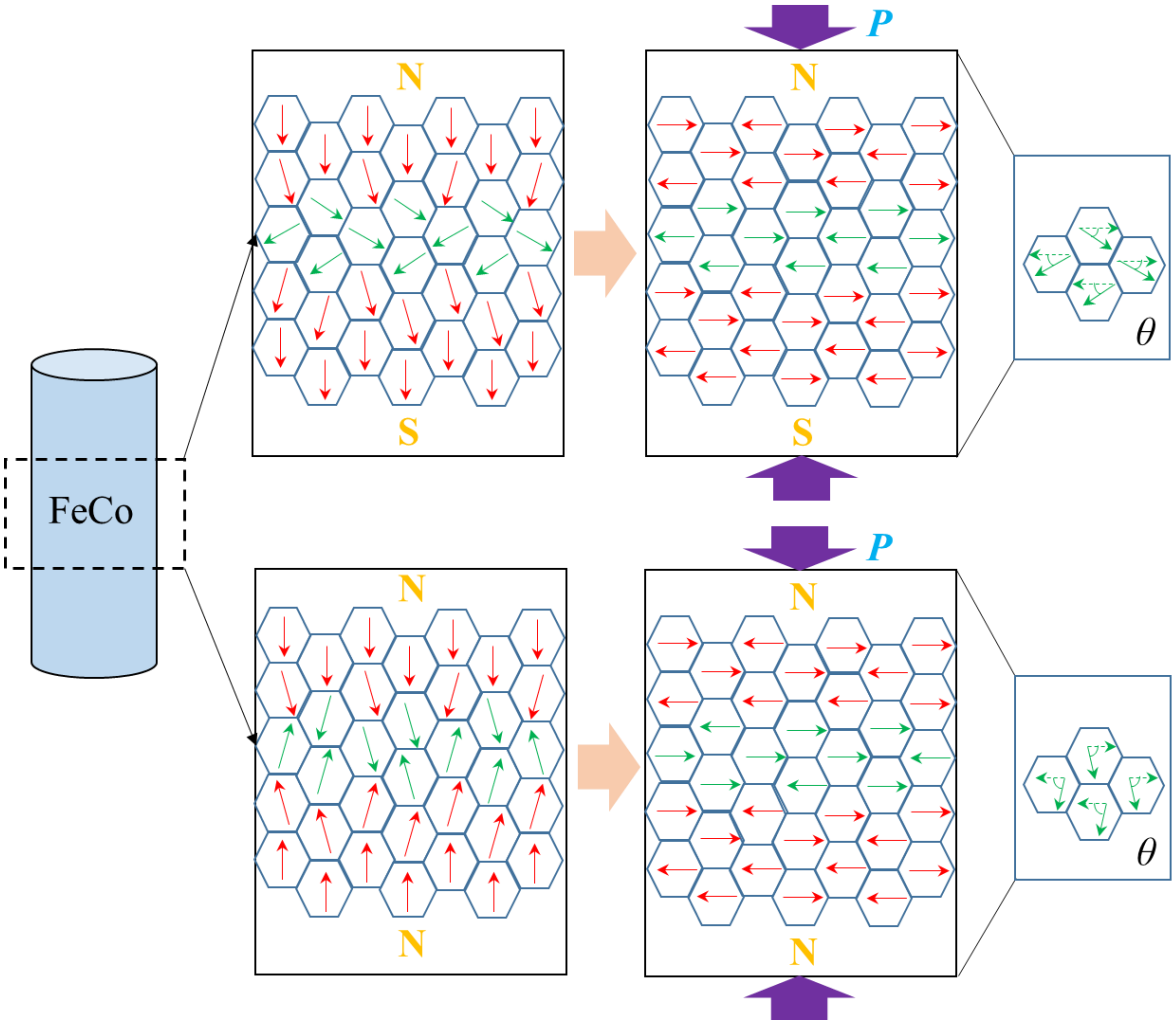


Fig. 5 Schematics for the magnetic domain rotation within the FeCo/AlSi composite in the N-S and N-N modes

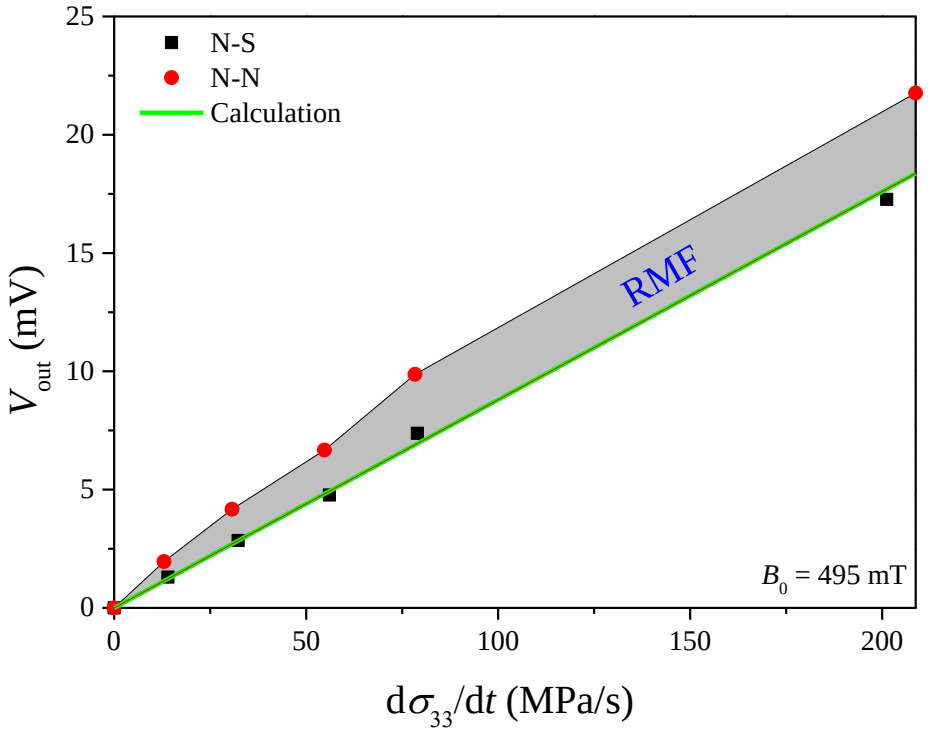


Fig. 6 Comparison of the output voltages for the FeCo/AlSi composite between the experiment and calculation